Harmful Algae 119 (2022) 102334

Contents lists available at ScienceDirect

Harmful Algae

journal homepage: www.elsevier.com/locate/hal

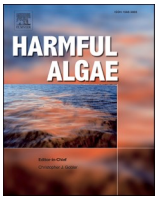

Assessing a model of Pacific Northwest harmful algal bloom transport as a decision-support tool

Hally B. Stone [a,1,*], Neil S. Banas [b], Parker MacCready [a], Vera L. Trainer [c], Daniel L. Ayres [d], Matthew V. Hunter [e]

[a] School of Oceanography, University of Washington, 1503 NE Boat St., Box 357940, Seattle, WA 98195, USA
[b] Department of Mathematics & Statistics, University of Strathclyde, 26 Richmond St., Glasgow, G1 1XH, UK
[c] Environmental and Fisheries Science Division, National Marine Fisheries Service, Northwest Fisheries Science Center, National Oceanic and Atmospheric Administration, 2725 Montlake Blvd. E., Seattle, WA 98112, USA
[d] Washington Department of Fish & Wildlife, 48 Devonshire Rd., Montesano, WA 98563, USA
[e] Marine Resources Program, Oregon Department of Fish & Wildlife, 2001 Marine Dr. Suite 120, Astoria, OR 97013, USA

ARTICLE INFO

Editor: Dr Holly Bowers

Keywords:
Harmful algal blooms
Pseudo-nitzschia
ROMS
Ocean observing
Ecological forecasting
Particle tracking

ABSTRACT

In the Pacific Northwest, blooms of the diatom Pseudo-nitzschia (*PN*) sometimes produce domoic acid, a neurotoxin that causes amnesic shellfish poisoning, leading to a Harmful Algal Bloom (HAB) event. The Pacific Northwest (PNW) HAB Bulletin project, a partnership between academic, government, and tribal stakeholders, uses a combination of beach and offshore monitoring data and ocean forecast modeling to better understand the formation, evolution, and transport of HABs in this region. This project produces periodic Bulletins to inform local stakeholders of current and forecasted conditions. The goal of this study was to help improve how the forecast model is used in the Bulletin's preparation through a retrospective particle-tracking experiment. Using past observations of beach *PN* cell counts, events were identified that likely originated in the Juan de Fuca eddy, a known *PN* hotspot, and then particle tracks were used in the model to simulate these events. A variety of "beaching definitions" were tested, based on both water depth and distance offshore, to define when a particle in the model was close enough to the coast that it was likely to correspond to cells appearing in the intertidal zone and in shellfish diets, as well as a variety of observed *PN* cell thresholds to determine what cell count should be used to describe an event that would warrant further action. The skill of these criteria was assessed by determining the fraction of true positives, true negatives, false positives, and false negatives within the model in comparison with observations, as well as a variety of derived model performance metrics. This analysis suggested that for our stakeholders' purposes, the most useful beaching definition is the 30 m isobath and the most useful *PN* cell threshold for coincident field-based sample *PN* density estimates is 10,000 *PN* cells/L. Lastly, the performance of a medium-resolution (1.5 km horizontal resolution) version of the model was compared with that of a high-resolution (0.5 km horizontal resolution) version, the latter currently used in forecasting for the PNW HAB Bulletin project. This analysis includes a direct comparison of the two model resolutions for one overlapping year (2017). These results suggested that a narrower, more realistic beaching definition is most useful in a high-resolution model, while a wider beaching definition is more appropriate in a lower resolution model like the medium-resolution version used in this analysis. Overall, this analysis demonstrated the importance of incorporating stakeholder needs into the statistical approach in order to generate the most effective decision-support information from oceanographic modeling.

1. Introduction

In the U.S. Pacific Northwest, harmful algal bloom (HAB) species in the genus *Pseudo-nitzschia* (*PN*), a type of diatom, produce domoic acid (DA), a neurotoxin that causes amnesic shellfish poisoning. DA is easily transferred up the food chain and can have severe or fatal effects

* Corresponding author.
E-mail address: hally.stone@noaa.gov (H.B. Stone).
[1] Present address: 1335 East-West Highway, Silver Spring, MD 20910

https://doi.org/10.1016/j.hal.2022.102334
Received 9 May 2022; Received in revised form 2 September 2022; Accepted 16 October 2022
Available online 29 October 2022

through the syndrome known as amnesic shellfish poisoning in seabirds, marine mammals, and humans (Lefebvre et al., 2002), and recent studies show a significant increase in amnesic shellfish toxin events associated with toxic *PN* blooms (D. M. Anderson et al., 2021; Hallegraeff et al., 2021). Given the dangerous health impacts, once DA is found on beaches where either commercial or recreational fishing occurs, these beaches are closed to activities such as shellfish harvest or fishing. These closures can significantly and negatively affect people whose livelihoods rely on these fisheries, including people within the commercial fishing industry itself and people within the tourism industry (Ritzman et al., 2018). Historical data of *PN* and DA on beaches suggests that there are years with numerous beaching events, and years with very few (e.g., McCabe et al. (2016); McKibben et al. (2017)). Ocean-atmosphere climate variability could explain some of the differences in HAB arrival in the nearshore coastal zone (hereafter termed "beaching events"), with warm anomalies associated with the Pacific Decadal Oscillation (PDO) and El Niño-Southern Oscillation (ENSO) correlated with *PN* beaching events in the Pacific Northwest (McCabe et al., 2016; McKibben et al., 2017).

In the Pacific Northwest, *PN* blooms generally originate in known offshore hotspots: the Juan de Fuca Eddy (approximate location correspond to the black dotted square feature in Fig. 1) in the summer and early fall (MacFadyen et al., 2005; Trainer et al., 2002, 2009) and Heceta Bank typically in the winter and early spring (Hickey et al., 2013). Both of these hotspots are retentive regions with appropriate supply of nutrients during some or all of the year. For *PN* cells to reach the coast from either of these retentive regions, enough *PN* cells must first accumulate at these offshore sites for a bloom to form. Then, this bloom must escape the retentive sites and travel to the coast. These steps require specific wind conditions. In the Juan de Fuca eddy, *PN* cells must first accumulate in the eddy under a balance of weak upwelling-favorable and downwelling-favorable winds. Next, *PN* cells escape the eddy under upwelling-favorable winds (MacFadyen et al., 2005, 2008; MacFadyen and Hickey, 2010). Finally, downwelling-favorable winds transport *PN* cells to the coast (MacFadyen et al., 2005; MacFadyen and Hickey, 2010; Trainer et al., 2002). These dynamics can be further complicated by the Columbia River plume, which can act as both a conduit and as a barrier for *PN* cells to the coast (Banas et al., 2009; Giddings et al., 2014; Hickey et al., 2013). During wind reversals in the summer or fall, the northern branch of the Columbia River plume is pushed against the coast, acting as a barrier to *PN* cell access to the WA coast. However, during strong storms in the winter, the Columbia River plume can help transport *PN* cells up even farther north along the coast.

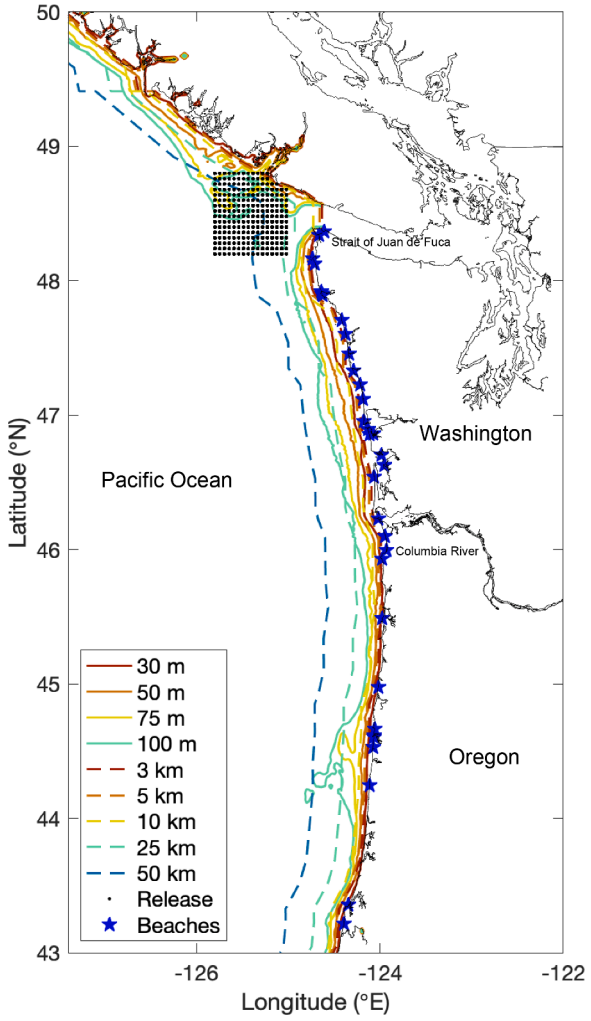

Fig. 1. Map of study location. Beach locations where *PN* were sampled are shown as blue stars, release points from the Juan de Fuca eddy for particle tracking experiments (described in Section 2.2) are plotted in black dots, and beaching definitions are plotted in colored lines. Beaching definitions based on isobath are plotted in solid lines and those based on distance offshore are plotted in dashed lines.

While many HAB events follow this pattern, there are some important nuances that add a layer of complexity to forecasting. Within the eddy itself, *PN* cells are not typically the dominant phytoplankton. They are often found within blooms of other types of diatoms, euglenoids, or dinoflagellates, usually making up no more than 17% of biomass within the Eddy (Trainer et al., 2009). Therefore, not every cell, or even most of the cells, that are transported to coastal beaches are *PN* cells. Additionally, the abundance of *PN* does not always correlate with concentration of DA, largely because there are many *PN* species that produce differing amounts of DA per cell, thus the presence of *PN* cells does not indicate presence of DA (Trainer et al., 2009). However, conservative risk levels of *PN* were established for the WA coast based on the historical record of DA in razor clams associated with the monitoring of *PN* and cellular DA. Specifically, these recorded events led to the establishment of threshold levels of 30,000 cells/L of large *P. australis*-type cells and 1 million cells/L of smaller *P. pseudodelicatissima*-type cells to trigger pre-emptive DA testing in seawater and razor clams by ORHAB and the Washington State Department of Health (Trainer and Suddleson, 2005). These conservative threshold levels established by ORHAB in 2005 have resulted in effective management by allowing for selective harvesting of clams from safe beaches (Varanasi et al., 2021), thereby avoiding any shellfish harvest recalls. Lastly, *PN* cells do not always originate in a known "hot spot" like the Juan de Fuca eddy. In six cruises spanning 2003 – 2006, which sampled the Juan de Fuca eddy and nearshore region, *PN* cells were observed both in the nearshore region and within the eddy, with some difference in *PN* species between regions, suggesting that these populations were unrelated (Trainer et al., 2009). Additionally, analysis of a coastwide HAB event in 2015 suggested that these *PN* originated from a diffuse offshore source rather than one of the usual "hot spots" sites such as the Juan de Fuca eddy or Heceta Bank (McCabe et al., 2016).

Given the huge economic losses that can result from fishery closures in the region, understanding when and where a HAB event will occur can help minimize the collateral damage that accompanies last-minute changes of plans due to an unexpected HAB event, such as suddenly having to close a beach right before a big razor clamming weekend, as well potentially avoid unnecessary closures. The Pacific Northwest (PNW) HAB Bulletin project, a partnership between academic, government, and tribal stakeholders, uses a combination of monitoring programs and modeling to better understand the formation, evolution, and transport of HABs in this region (Varanasi et al., 2021). In addition, this project produces periodic bulletins to inform local stakeholders of current and forecasted conditions. These Bulletins make HAB risk recommendations based on expert synthesis of observations including *in situ* sampling of *PN* cells, quantification of particulate (cellular) DA and razor clam DA, wind and surface current patterns, satellite chlorophyll

concentrations, and river discharge, as well as relevant Pacific Ocean indices, and marine weather forecasts. In addition, the PNW HAB Bulletin uses 72-h model forecasts of *PN* transport from the Juan de Fuca Eddy and Heceta Bank. One goal of this paper was to analyze particle tracks, combined with a variety of beaching and event criteria, to improve the forecasting capabilities of the model. With improved forecasting, it is possible that alerts could be issued to managers about future HAB events with enough notice to open a beach early for harvest before the HAB reaches the coast, which could be extremely beneficial to both the economy and to those whose livelihoods rely on the commercial or recreational fishing industries.

In this study, *in situ* beaching data combined with particle tracking experiments were used with the goal of improving the effectiveness of the forecasting model for HABs that originate in the Juan de Fuca eddy. As part of this analysis, various definitions of modeled HAB beaching and observational thresholds were tested to identify which criteria best matched observations and therefore were most appropriate for use in the forecasting model. Lastly, results from an older medium-resolution version of the model were compared with the newer high-resolution version of the model, the latter which is currently used for forecasting for the PNW HAB Bulletin.

2. Methods

2.1. Beach observations

Abundance of PN was determined in surface whole water samples collected from the surf zone at 45 beaches (shown as blue stars in Fig. 1) in Washington and Oregon spanning 2000 – 2020 using methods described in Trainer and Suddleson (2005) and McKibben et al. (2015). In Washington, beach observations were conducted by the Olympic Region Harmful Algal Bloom (ORHAB) partnership (http://depts.washington.edu/orhab/). In Oregon, past beach observations were conducted by Oregon Department of Fish and Wildlife as part of the Monitoring Oregon Coastal Harmful Algae (MOCHA 2007-2012) project and continue today supported by the Monitoring and Event Response for Harmful Algal Blooms (MERHAB 2017-2022) program as part of the PNW HAB Bulletin project. This paper focused on observations north of the Columbia River mouth, where beach sampling was most consistent (as demonstrated in Fig. 2), during the summer-autumn upwelling period (June 1 – Fall transition).

PN abundance from 2000 to 2020 at 45 beaches in Washington and Oregon is shown in Fig. 2. In this record, it was evident that large events with high cell counts infrequently affected large areas of the coast, typically occurring no more than a couple of times a year. While the observational record lasted many years, sampling at individual beaches was sporadic, leaving large gaps in the record, particularly in Oregon.

2.2. Particle tracking experiments

To test whether the model captures the proposed mechanism of transport from the Juan de Fuca eddy, and assess the skill of the PNW Bulletin forecasting system, particle release experiments were conducted for three different versions of the model: first, a high-resolution version of the LiveOcean series spanning 2017 – 2021, as well as two other versions that use the medium-resolution grid of the *Cascadia* model, with output spanning 2003 – 2009 (PNWTOX series) and 2013 – 2018 (part of the LiveOcean series). The only difference between the two versions of the medium-resolution model is that due to the NCOM global model (Navy Coastal Ocean Model; Barron et al., 2006, 2007) transitioning to the HYCOM global model (HYbrid Coordinate Ocean Model; https://www.hycom.org/) in 2013, the earlier years (2003 – 2009) used NCOM for the open ocean boundary initialization and forcing while the later years (2013 – 2017) used HYCOM, which has a slightly higher resolution. This difference resulted in only small variations between the two models, which made them effectively the same model, so their output was treated (and referred to) as one version for this analysis. These models were developed by the University of Washington Coastal Modeling Group (Giddings et al., 2014; Sutherland et al., 2011) using the Regional Oceanic Modeling System (ROMS; Shchepetkin and McWilliams (2005)). The model domain includes the Salish Sea and coastal ocean of Washington, Oregon, and southern British Columbia,

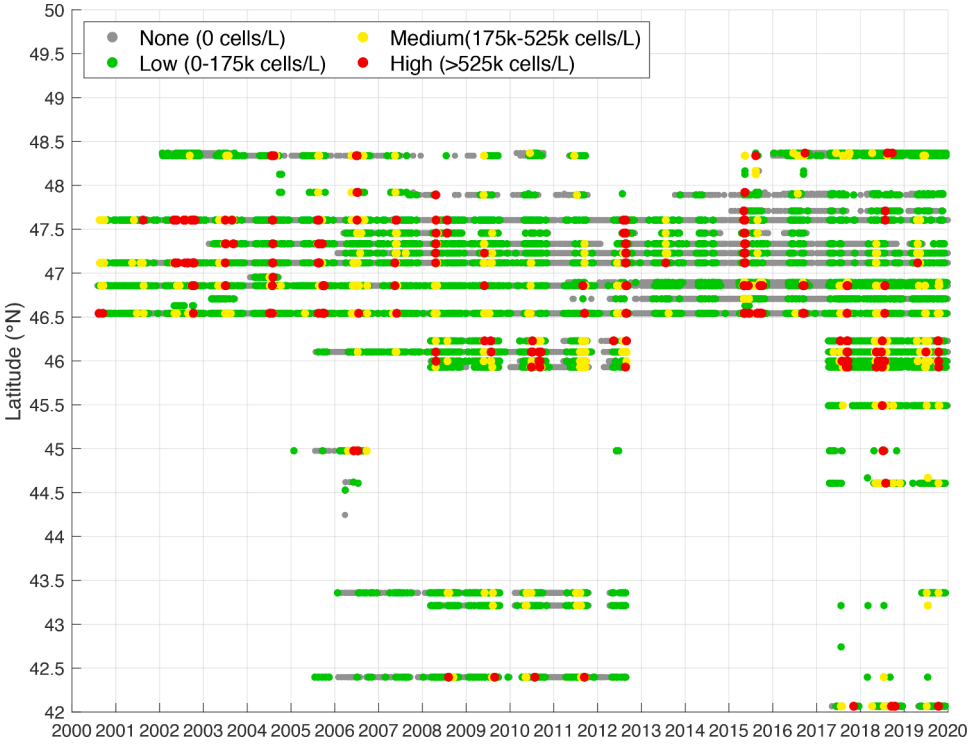

Fig. 2. Beach observations of *PN* abundance (see legend for ranges) from 2000 – 2020 at 42N – 50N latitude. White areas indicate gaps in sampling.

spanning 42N to 52N, -130E to -122E (Fig. 1). The horizontal resolution of the model over the slope and shelf is 500 m and expands to a maximum of 3 km offshore. The model uses realistic river, atmospheric, and tidal forcing, and open ocean boundary condition fields from other models constrained by observations or short-term forecasts. Further details about the high-resolution version of the LiveOcean model and its validation can be found in MacCready et al. (2021). The effect of model resolution was also tested by performing similar experiments in earlier versions of the model in which the grid size was coarser by a factor of three. These experiments spanned different years: 2003 – 2009 and 2013 – 2018 (dictated by the time span of the projects for which they were developed). Model details for these lower resolution experiments are given in Davis et al. (2014), Giddings et al. (2014), Siedlecki et al. (2015), and Brasseale et al. (2019). The comparisons were not, however, a pure test of change in resolution, because they are for different time periods (aside from 2017 during which they overlap) and different sources of forcing fields, so the results can only be suggestive of the improvements gained due to higher resolution.

Particles were released at the surface within the typical extent of the Juan de Fuca eddy (48.2 – 48.8N; 125.8° – 125W) with release points every 0.052° in longitude and 0.04° in latitude (black dots, Fig. 1). Release points that were above the 30 m isobath were removed, resulting in 247 release points in the high-resolution version of the model. One particle was released from each release point every 2 days from June 1 to the Fall transition from 2017 – 2019, resulting in approximately 13,832 particle releases per year, though the number depended on the date of each Fall transition, based on the method of Barth et al. (2007) and Pierce et al. (2006). Particles were released from the Juan de Fuca eddy only between June 1 and the fall transition date, which captured the major razor clamming season dates. This release period was chosen because the Juan de Fuca eddy is a seasonal feature that is typically present during the upwelling season (Denman and Freeland, 1985; Freeland and Denman, 1982; Freeland and McIntosh, 1989; MacFadyen et al., 2005; MacFadyen and Hickey, 2010). Once released, the surface-trapped particles were tracked with hourly time steps and output saved daily for up to 30 days, or until they moved outside the model boundaries or ‘‘grounded’’ on land, defined as being close enough to land that a bilinear interpolation of the ROMS land mask (1 for ocean, 0 for land) at its location was less than 0.5 (Banas et al., 2015; Stone et al., 2018). When a particle is “grounded”, it often indicates that it became stuck in a model grid cell that is more land than ocean, so said particle is no longer tracked. The same particle release experiment was repeated in the medium resolution version of the model for 2004 – 2007 and 2013 – 2017, and tidally averaged model output was used for this particle release experiment. Due to the difference in resolution, after release points above the 30 m isobath were filtered out, there were 246 release points for the experiments in the medium-resolution version of the model (1 fewer than in the experiments in the high-resolution model), resulting in an average of 15,799 particles released each year for 2004 – 2007; 2013 – 2017.

2.3. Beaching definitions and observational thresholds

With the particle tracks, a variety of beaching definitions were tested, i.e., what counts as a “beached particle”, within the model to determine which definition best captured the observed beaching of *PN* cells that originated in the Juan de Fuca eddy. The dynamics of the inner shelf, including cross-shelf transport across the surf zone, are not resolved in the model, so it was assumed for forecasting purposes that any time a particle got within a certain distance or passed a certain isobath, there was a high probability of *PN* cells being present at the beach, even if the paths of these particles continued moving south, parallel to the coast in the model, and that the particle was not considered “grounded” on land within the model. For beaching definitions, both isobath-based definitions (30, 50, 75, and 100 m isobaths) and definitions based on distance offshore (3, 5, 10, 25, and 50 km offshore; Fig. 1) were tested. These beaching definitions can be thought of as statistical proxies for inner-shelf and surf-zone physics that are missing from our regional-scale ocean model. In this paper, output from June 1 through the Fall transition for 2017 – 2019 in the high resolution model, and for 2004 – 2007 and 2013 – 2017 in the medium resolution model and at beaches above the Columbia River mouth (46N – 48N) were used to test these definitions, as most of the observations of *PN* cells from the Juan de Fuca eddy occur during the late summer and early fall (Giddings et al., 2014; MacFadyen et al., 2005; Trainer et al., 2002, 2009).

Observational PN cell density thresholds (10 *PN* cells/L, 100 *PN* cells/L, 1,000 *PN* cells/L, 10,000 *PN* cells/L, 100,000 *PN* cells/L, 175,000 *PN* cells/L, 525,000 *PN* cells/L, and 1,000,000 *PN* cells/L) were also tested as criteria for beaching events. These thresholds, i.e., what abundance of *PN* cells count as a beaching event in the observations, were chosen based on the observational threshold used for the California Harmful Algal Risk Mapping (C-HARM) system to establish whether there was a *PN* bloom (Anderson et al., 2016), 10,000 *PN* cells/L, as well as the thresholds used in the PNW HAB Bulletin to describe the severity of beached HAB measurements, where 175,000 *PN* cells/L is the threshold between low and medium cell counts (plotted in yellow in Fig. 2) and 525,000 *PN* cells/L is the threshold between medium and high cells counts (plotted in red in Fig. 2).

2.4. Skill assessment

To address the model skill associated with each of the beaching definitions and observational thresholds outlined in Section 2.3, locations and timings of beached particles were compared with observed *PN* cell counts at Washington beaches. For this calculation, the daily beached particle count was compared with observed beach cell counts from the proceeding, corresponding, and following day, i.e., ±1 day, for each 0.125° latitude bin across all analyzed summers (from June 1 through the Fall transition). Again, as discussed in the Introduction, it is important to note that in this study, model particles originated only from the Juan de Fuca Eddy and therefore were unlikely to capture the transport pathways of *PN* cells from regions outside the eddy. Thus, even a perfect transport-based forecast may under-predict beach events.

Daily particle transport model results were compared with *PN* abundance (measured within one day before or after the particle results) for each 0.125° of coastline from the mouth of the Columbia River north to the mouth of the Strait of Juan de Fuca, and were then categorized as “true positive” (at least one model particle beached and observed *PN* abundance was above the threshold), “true negative” (no model particles beached and *PN* abundance was below the threshold), “false positive”, and “false negative”. In testing each of the observational thresholds, there was no difference between *PN* cell counts observed at each beach; instead, analysis focused on whether or not the observed cell count was greater or less than the tested threshold. For example, if the tested threshold was 10,000 *PN* cells/L, then any measurement of at least 10,000 *PN* cell/L at a beach, including all green, yellow, and red events (shown in Figs. 2 and 3), counted as a positive observation and any measurement of less than 10,000 *PN* cells/L at a beach counted as a negative observation. From here, a variety of performance metrics including accuracy, probability of detection, false alarm ratio, probability of false detection, and bias score (Table 1) were calculated following Anderson et al. (2010, 2016). The relative importance of each of these metrics was dependent on the needs of the stakeholder. For example, in the analysis of various observed *PN* bloom thresholds used in the C-HARM system, minimizing the false alarm ratio (FAR) compared to probability of detection (POD) was important to stakeholders, which resulted in an overall accuracy of 43%, though the best performing threshold had an overall accuracy of 67% (Anderson et al., 2016).

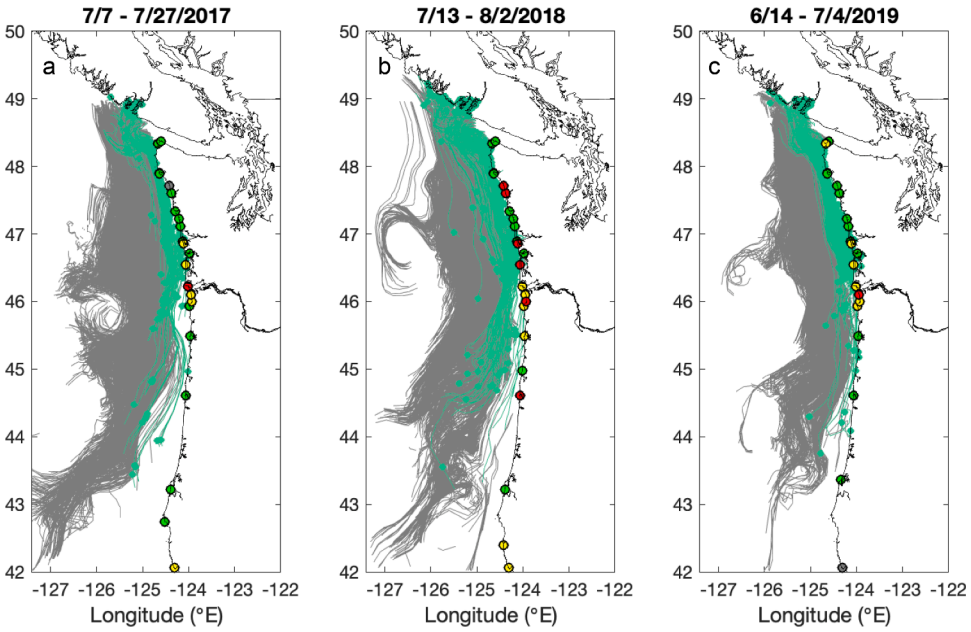

Fig. 3. Maps of particle tracks for events identified in observations from 2017, 2018, and 2019. In each figure, particles that beached within ±10 days of each identified event (defined as passing the 30 m isobath, in this case) are plotted in green, while particles that did not beach during this time period are plotted in grey. Observed *PN* cell counts are plotted at sampled beaches (grey, green, yellow, and red circles), indicating the maximum measured cell count over the 20-day period, using the same scale as in Fig. 2.

Table 1
Performance metrics and their calculations, following (Anderson et al., 2010, 2016).

Performance Metric	Calculation	Range
Accuracy	$\frac{true\ positives\ +\ true\ negatives}{total}$	0 – 1 (1 is best)
Probability of Detection (POD)	$\frac{true\ positives}{true\ positives + false\ negatives}$	0 – 1 (1 is best)
False Alarm Ratio (FAR)	$\frac{false\ positives}{true\ positives + false\ positives}$	0 – 1 (0 is best)
Probability of False Detection (POFD)	$\frac{false\ positives}{true\ negatives + false\ positives}$	0 – 1 (0 is best)
Bias Score	$\frac{true\ positives + false\ positives}{true\ positives + false\ negatives}$	0 – ∞ (1 is best)

3. Results

3.1. Particle tracking experiments

Using the observational record, upwelling-season beaching events with *PN* abundance were identified for 2017, 2018, and 2019, the years for which there was high-resolution model output. Using the particle tracking experiments, these events were recreated using the model (Fig. 3). In each of these plots, particle tracks were mapped from 10 days before the identified event to 10 days after, with particles that beached plotted in green and particles that did not beach plotted in grey. In all of the maps shown in Fig. 3, "beached" particles were any particles that crossed the 30 m isobath at any point along their track. The maximum observed cell counts at beaches in the region were also plotted on the maps.

In all of these scenarios, there were many particles that were transported equatorward along the shelf and slope, though the alongcoast extent of their transport varied among events. It was also evident that most particles passed very close to the coast in the immediate vicinity of their release near the mouth of the Strait of Juan de Fuca, and then moved down the coast at varying distances offshore that may not be considered to be "beached" by the tested definition farther south. For example, the particle paths in the 2019 event (Fig. 3c) stayed on the shelf and would likely be considered beached as far south as 43.5N, while the particle paths in the 2017 event (Fig. 3a) primarily moved off the shelf near the mouth of the Columbia River (~46N).

3.2. Model performance

To address the performance of each of the beaching definitions and observational thresholds outlined in Section 2.3, the fraction of true positives, true negatives, false positives, and false negatives were counted for each 0.125° latitude bin across all analyzed summers (from June 1 through the Fall transition). This analysis utilized particle tracking results from all high-resolution version of the model runs spanning 2017 – 2019. The results of this analysis showed the performance of each beaching definition across observational thresholds (Fig. 4).

The optimal (or, most useful for our stakeholders), combination of beaching definition and observational threshold maximized true positives while minimizing false negatives and false positives in order to accurately forecast when a toxic HAB event would potentially arrive on the beach. The overall trend for all beaching definitions was that true positives and false negatives were highest at low observational thresholds, while true negatives and false positives exhibited the opposite relationship and were highest at high observational thresholds. The isobath-based beaching definitions (solid lines, Fig. 4) generally fell in the middle of the distance-based beaching definitions (dashed lines, Fig. 4) across all observational thresholds. Generally, the wider beaching definitions (cool colors - greens and blues, Fig. 4) resulted in more true positives and false positives, while the narrower beaching definitions (warm colors - reds and yellows, Fig. 4) resulted in more true negatives and fewer false positives across all observational thresholds. The 30 m isobath beaching definition (solid red line, Fig. 4) presented a good balance between maximizing true positives while minimizing false negatives and false positives, with the optimal balance obtained using an observational threshold of 10,000 *PN* cells/L (red dot in Fig. 4), though the performance of the 10,000 *PN* cells/L threshold is shown more clearly in Figs. 5 and 6. From the distance-based beaching definitions, the 10 km offshore beaching threshold also performed well, closely mirroring the results from the 30 m isobath beaching definition (dashed yellow line, Fig. 4).

Under most of these beaching definitions, the accuracy of the model prediction as defined in Table 1 decreased with increasing observational threshold, although this trend diminished as beaching definition narrowed (warm colors), and the narrowest beaching definitions (3 and 5 km offshore, dashed red and orange lines, respectively) exhibited the opposite trend. Again, the best performing beaching definitions across

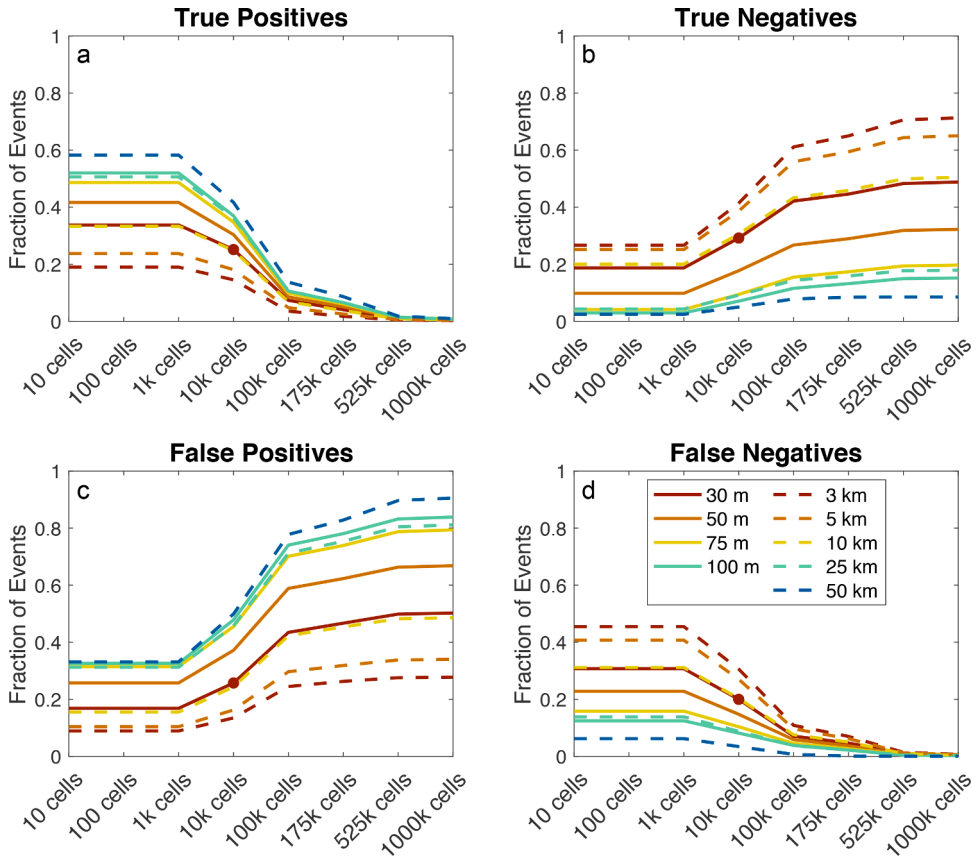

Fig. 4. Statistics for each beaching definition across all observational thresholds for 2017 – 2019: fraction of true positives (a), fraction of true negatives (b), fraction of false positives (c), and fraction of false negatives (d). Solid lines represent isobath-based definitions and dashed lines represent distance offshore-based definitions as in Fig. 1. The red dot represents the results for the most useful beaching definition (30 m isobath) and observational threshold (10,000 cells/L).

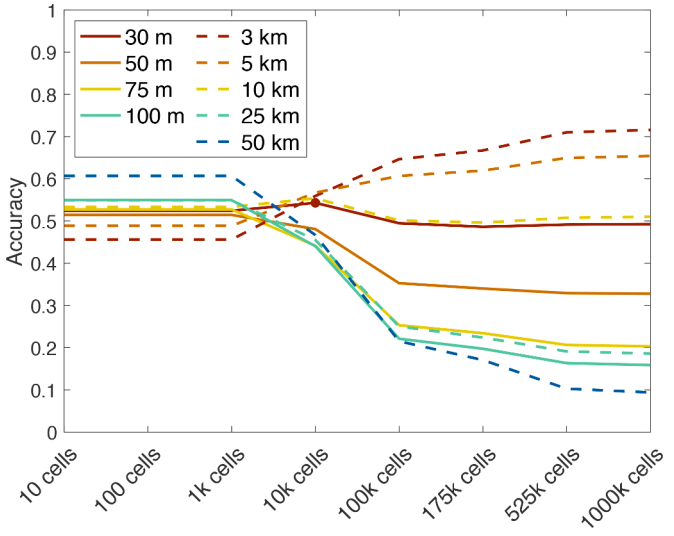

Fig. 5. Accuracy of each beaching definition across all observational thresholds for 2017 – 2019. Beaching definitions are depicted by colored lines (see legend) with solid lines representing isobath-based definitions and dashed lines representing distance offshore-based definitions. The red dot represents the results for the optimal beaching definition (30 m isobath) and observational threshold (10,000 cells/L).

all observational thresholds were the 30 m isobath and 10 km offshore (solid red line and dashed yellow line, respectively, Fig. 5), with an accuracy of about 55% for both beaching definitions at the same optimal observational threshold, 10,000 *PN* cells/L (red dot, Fig. 5). For comparison, the best overall accuracy score of the C-HARM system was 67%, though the threshold that performed best considering their goal to optimize FAR compared to POD had an accuracy of 43% (Anderson et al., 2016). While the results from the 30 m isobath definition closely matched the results from the 10 km offshore definition, the 30 m isobath definition was chosen for further analysis. The isobath-based definition better represents the geometry of the near-shore region, which would inform the cross-shelf circulation, while a set distance offshore could include a variety of water depths and would be less indicative of the cross-shelf circulation. The performance of the 30 m isobath beaching definition across observational thresholds was evaluated further by calculating the remaining metrics outlined in Table 1 (Fig. 6).

Based the goals of the C-HARM system (Anderson et al., 2016), the optimal combination of beaching definitions and observational thresholds for this model would maximize accuracy and probability of detection (POD), minimize the false alarm ration (FAR) and probability of false detection (POFD), and result in a bias score close to 1. With the 30 m isobath beaching definition, generally, the lower observational thresholds had slightly higher POD and accuracy scores, while the higher observational thresholds had the opposite (Fig. 6). However, based on how our stakeholders use our forecast to direct sampling (see Discussion), maximizing POD was more important than minimizing FAR and POFD because maximizing POD included minimizing false negatives. Therefore, the most useful observational threshold overall was judged to be 10,000 *PN* cells/L, where POD was maximized and POFD was minimized. Still, the prediction did perform comparably well at lower observational thresholds as well and 1,000 *PN* cells/L is a close second-best with a slightly lower POD and slightly lower PFOD. Further, these similar results at lower thresholds highlight the value of an "any

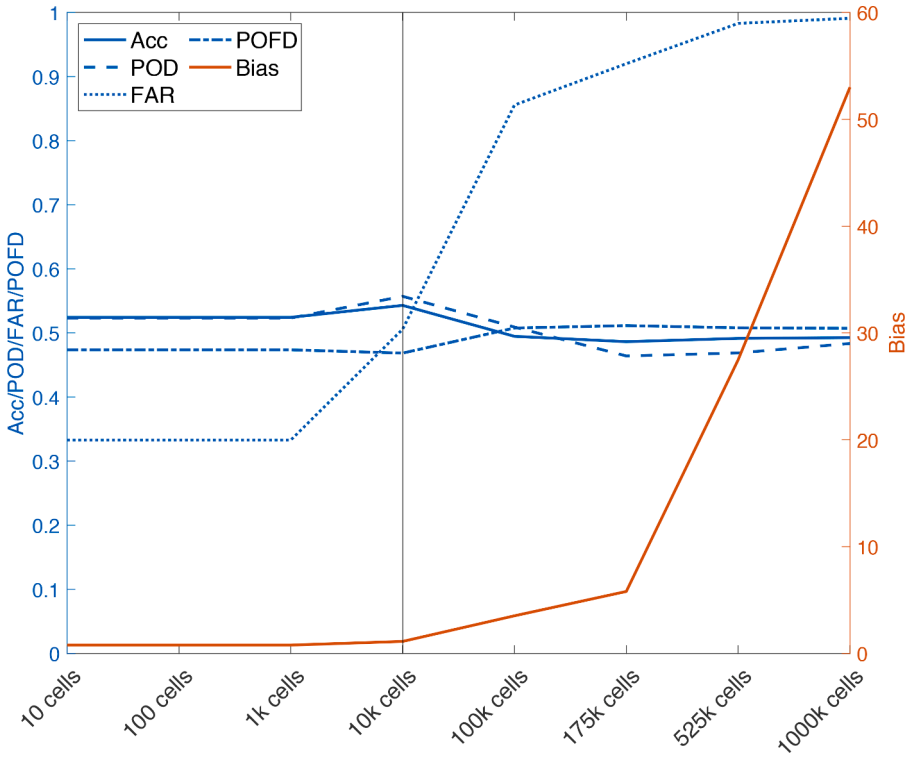

Fig. 6. Metrics for the 30-m isobath beaching definition across all observational thresholds for 2017 – 2019. Accuracy (Acc), Probability of Detection (POD), False Alarm Ratio (FAR), and Probability of False Detection (POFD) are in blue lines of various styles (left y-axis; see legend) and Bias is plotted in orange (right y-axis). The vertical grey line represents the results for the optimal observational threshold (10,000 *PN* cells/L).

cell beaching" threshold over a "big event" threshold (see Discussion). Overall, these results illustrated the importance of considering a suite of metrics as well as stakeholder needs in model evaluation.

3.3. Comparison of the medium-resolution and high-resolution versions of the model

Lastly, the existence of an older model version that overlaps with many of the observations as well as one year of the newer model version provided a unique opportunity to compare their performances, both in 2017 where they overlap and as a whole using output from 2004 – 2007 to 2013 – 2017 in the medium-resolution version and output from 2017 to 2019 in the high-resolution version (Figs. 7 and 8, Table 2). The most notable differences in these two versions were evident in the maps of particle tracks surrounding the identified event in 2017, with the results from the medium-resolution version shown in Fig. 7f and those from the high-resolution version shown in Fig. 3a.

In the medium-resolution version of the model, particles were closest to the coast near their release point and then streamed down along the coast at distances that would not be considered "beached" by most of the tested beaching definitions farther south (Fig. 7). However, the high-resolution version exhibited stronger cross-shelf dispersion, particularly within the 46N – 47N band, as was evident in the particle tracks that flow closer to the coast as they moved southward, with cross-shelf movement evident in their particle tracks (Fig. 3). Accordingly, there were many more particles that beached in the high-resolution version than those that beached in the medium-resolution version.

Given the weaker cross-shelf dispersion in the medium-resolution version of the model, wider beaching definitions were also tested based on isobath and compared with the results from the high-resolution version of the model. As done previously, the fraction of true positives, true negatives, false positives, and false negatives were calculated for each beaching definition (Fig. 8). These results included June 1 through the Fall transition for 2004 – 2007 and 2013 – 2017 in the medium-resolution version of the model and for 2017 – 2019 in the high-resolution version of the model. All scenarios used an observational threshold of 10,000 *PN* cells/L.

Results showed that the medium-resolution version captured more true negatives and more false negatives (orange bars, Fig. 8b, d) than did the high-resolution version (blue bars, Fig. 8b, d), decreasing in both versions as the beaching definition widened. Conversely, the high-resolution version captured more true positives and more false positives (blue bars, Fig. 8a, c) than did the medium-resolution version (orange bars, Fig. 8a, c), increasing in both versions as the beaching definition widened. Overall, these results suggested that using a wider beaching definition, like the 50 m or 75 m isobath, in a lower resolution model would result in a similar performance as was obtained with the higher-resolution model using the optimal beaching definition, the 30 m isobath.

For almost all performance metrics, the medium-resolution version did worse than the high-resolution version (Table 2). The only exception to this pattern was POFD, which was largely driven by the greater fraction of false positives in the high-resolution version than in the medium-resolution version. Notably, the POD score of the high-resolution version was almost double that of the medium-resolution version (Table 2).

4. Discussion

The current PNW HAB Bulletin is largely tailored to the needs of our stakeholders, including the managers of the Washington and Oregon recreational razor clam fisheries. Safely managing such a large fishery as the Washington recreational razor clam fishery that can have 25,000 to 30,000 harvesters in a four-hour low tide window, stretched over 58 miles of beaches, requires close consultation between fishery managers and human health experts. As such, Washington's recreational razor clam fishery is always closed unless it is specifically opened. In general, openers (open seasons) are purposefully limited to not more than one

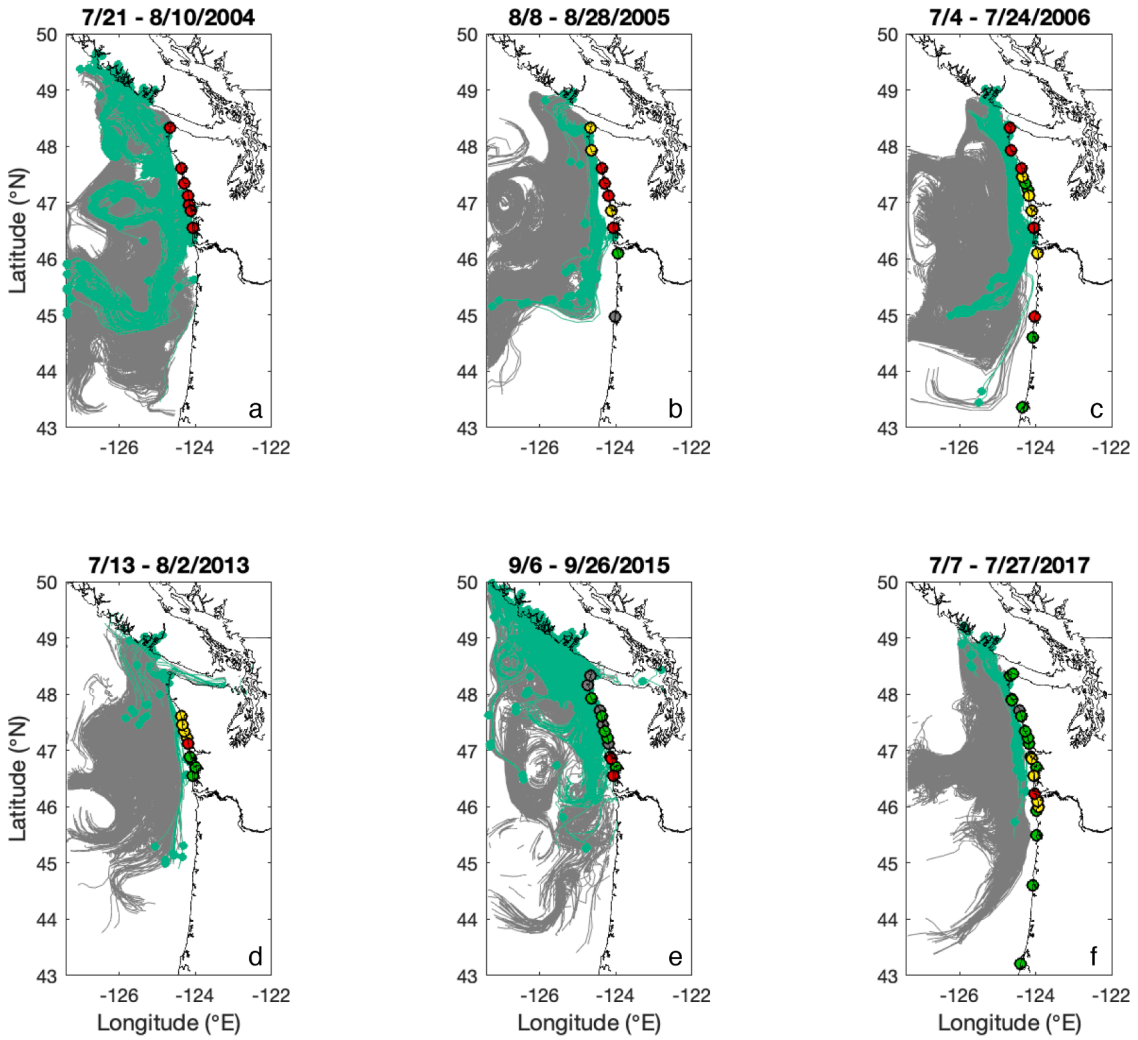

Fig. 7. Maps of particle tracks for the beaching events identified in (a) 2004, (b) 2005, (c) 2006, (d) 2013, (e) 2015, and (f) 2017 using the medium-resolution version of the model. In each figure, particles that beached within ±10 days of each identified event (defined as passing the 30 m isobath) are plotted in green, while particles that did not beach during this time period are plotted in grey. Observed cell counts are plotted at sampled beaches (grey, green, yellow, and red circles), indicating the maximum measured cell count over the 20-day period, using the same scale as used in Fig. 2.

Table 2
Performance metrics (defined in Table 1) for the high-resolution version of the model (2017 – 2019) and the medium-resolution version of the model (2004 – 2007; 2013 – 2017) using the 30-m isobath as a beaching definition and 10,000 *PN* cells/L as an observational threshold.

Performance Metric	Accuracy	POD	FAR	POFD	Bias
High-resolution version	0.54	0.56	0.51	0.47	1.13
Medium-resolution version	0.46	0.28	0.64	0.40	0.77

tide series (5 – 7 days) at a time. The fishery does not re-open until more razor clam samples are analyzed and found to be safe. In contrast, Oregon's razor clam fishery is generally always open unless it is specifically closed, although it has far fewer harvesters than Washington's does. Specifically, Clatsop Beach, the 18-mile stretch of coast northern end of the State, is open from October 1 through July 14, while the rest of the coast south of Clatsop Beach is open year-round. Washington's and Oregon's fishery managers do regular shore-side phytoplankton sampling to make sure that *PN* cells are not present in high levels in surf zone water collections and use the PNW HAB Bulletin and model forecast to design targeted sampling, as well as to add unplanned sampling if particles are forecasted to come ashore. Fishery managers then consult with the state's human health managers to determine if schedules for shellfish tissue testing need to be modified to ensure that biotoxins are still within safe levels for harvesting. To that end, both false positives and false negatives can be costly and should be minimized because while false positives can lead to wasted resources if they result in unplanned sampling, false negatives can lead to delays in targeted sampling and managers have to "play catch-up" unnecessarily.

The transport-based forecast described here resulted in numerous false positives, particularly in the high-resolution version of the model, consistent with the fact that the method relied only on the physics of the region and did not incorporate any prediction of whether there were *PN* cells in the offshore source region available to be transported. Because of this, it would be unwise to focus on metrics that weigh heavily on the false positives, like the false alarm ratio (FAR) and probability of false detection (POFD) (Table 1). In contrast, false negatives were more noteworthy because they highlighted flaws in the transport of particles onshore, as well as flaws in the assumption of the source of *PN* cells that beached, like if *PN* cells came from offshore rather than from the Juan de Fuca eddy.

In testing various observational thresholds, two regimes were apparent: "big events" of greater than 10,000 *PN* cells/L and "any cell beaching" of less than 10,000 *PN* cells/L. This regime split was most evident in Figs. 4–6, where results were similar for thresholds below 10,000 *PN* cells/L as well as similar for thresholds above 10,000 *PN*

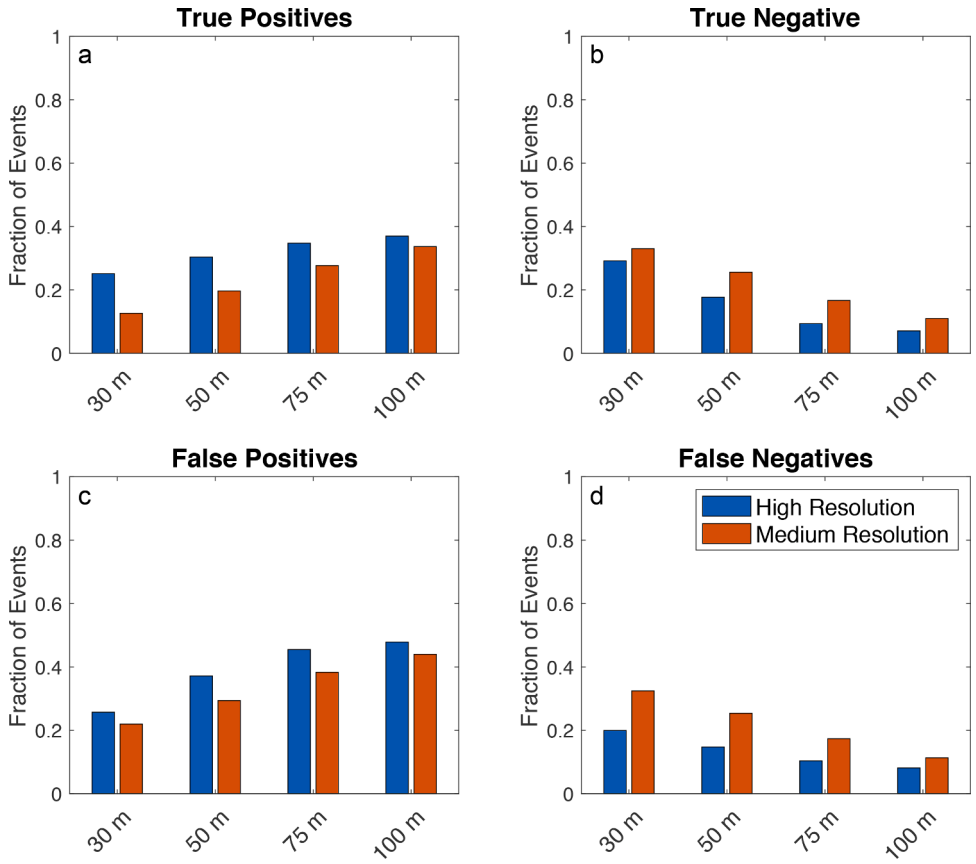

Fig. 8. Statistics for each isobath-based beaching definition with an observational threshold of 10,000 cells/L for 2017 – 2019 in the high-resolution version of the model (blue) and for 2004 – 2007; 2013 – 2017 in the medium-resolution version of the model (orange): (a) fraction of true positives, (b) fraction of true negatives, (c) fraction of false positives, and (d) fraction of false negatives.

cells/L. Since our stakeholders use the model's forecast and the PNW HAB Bulletin to understand oceanographic trends that then potentially will direct further sampling to aid in their opening or closure decisions, not make their opening or closure decisions, it is more important for our model to be able to predict when and where some number of particles will beach rather than the magnitude of the event. One advantage of such a model is that "any cell beaching" predictions would allow fisheries managers to target specific areas for additional sample collection before re-opening a beach. Similarly, our analysis demonstrated that narrower beaching definitions were more useful predictively (as well as being more mechanistically accurate) than wider beaching definitions, regardless of whether a small or large observational threshold was used. However, if a wider beaching definition was used, it performed better with "any cell beaching" than with "big events" because "big events" were dominated by false positives and poor success at replicating reality, while "any cell beaching" was dominated by true positives and much greater success at replicating reality.

While there are more metrics to consider beyond accuracy alone, the accuracies for each of the beaching definitions and observational thresholds may seem unimpressive. They ranged from about 9% to 72% accuracy, with a convergence on about 45 – 55% accuracy between the 1,000 *PN* cells/L and 10,000 *PN* cells/L thresholds. It is important to note that that model accuracy is impacted by several modes of uncertainty, so 50% net accuracy is a product of a lack of knowledge about when a bloom in the Juan de Fuca eddy happens, a lack of knowledge about whether the bloom contains *PN*, and the error in the model dynamics and particle tracking choices that represent pathway from eddy to beach. Only the pathways from the eddy to the beaches were predicted, but the data tested against involves all three of these unknowns. However, there is an active effort to improve this aspect of the model by periodic deployment of an environmental sample processor (ESP) near the Juan de Fuca eddy. Incorporating a complementary sensor like an ESP that can detect the presence of toxic *PN* offshore could potentially significantly improve forecast performance.

The comparison of the results from the high-resolution version and the medium-resolution version of the model highlight the importance of accurate cross-shelf transport in the model, despite the fact that the dominant currents are along-shelf. The differences in cross-shelf dispersion (Figs. 3, 7) were likely the reason that the more realistic 30 m isobath beaching definition (the 30 m isobath approximates the beginning of the inner shelf where the surface and bottom layers interact (Lentz and Fewings, 2012)) performed better in the high-resolution version of the model than it did in the medium-resolution version. Why then is dispersive cross-shelf transport so much weaker in the medium-resolution version of the model? The most notable differences in model setup were that the higher-resolution version also had higher resolution in its open ocean boundary inputs as well as its wind forcing, and included many more coastal rivers (18, as opposed to the Columbia River alone). Given the distance from the shelf to the open-ocean boundaries, it is unlikely that the boundary forcing was responsible for the improved cross-shelf dispersion in the high-resolution version. Better representation of freshwater input from many small sources may well be the explanation. Banas et al. (2009) found that the Columbia River plume and its interaction with variable winds increases cross-shelf dispersion, resulting in 25% more export across the shelf when it was included in the model than when it was not, and the addition of many small, but numerous, coastal river plumes might have a similar effect. It is also possible that the increased dispersion in the newer version of the model might be caused by the higher horizontal resolution itself, if it allows the model to better resolve the influence of submesoscale

processes and internal tides in promoting cross-shelf dispersion (e.g., Brink (2016); Davies and Xing (2001); Lévy et al. (2012); Noble et al. (2009)). Further analysis, including comparison of salinity and cross-shelf velocity over the shelf, could help untangle these influences.

While it is true that the higher resolution version of the model performed better than the lower resolution version of the model, as is evident in the performance metrics for both versions of the model using the 30 m isobath and 10,000 *PN* cells/L threshold that are outlined in Table 2, it is important to consider the cost of switching to a higher resolution model. For example, the main difference between the model versions is that LiveOcean (the higher resolution version of the model) has about three times finer resolution horizontally than does PNWTOX (the lower resolution version of the model), amounting to about 10 times more grid points. Because there is now more computational power available to run LiveOcean, it takes approximately the same amount of time (10 days) to produce 1 year of model output as it did for PNWTOX. The value added to the forecast on the shelf may not alone have been enough to warrant the model upgrade; however, the higher resolution of LiveOcean is critical for its performance in the Salish Sea and coastal estuaries. So, while the improvement to the performance of this forecasting model alone may not have been worth the cost to upgrade, the model's performance for its other uses made the upgrade worthwhile.

Despite the role that rivers may play in facilitating more cross-shelf flow within the high-resolution version of the model, the Columbia River plume largely acts as a barrier between the Juan de Fuca Eddy and the coast, particularly during downwelling-favorable winds. These effects were evident in the region immediately north of the Columbia River mouth (~46.25N) where a lot of false negatives were found, i.e., where there were no particles beaching in the model but *PN* cells were observed, a pattern also observed in other modeling studies that investigated the influence of the Columbia River plume (Banas et al., 2009; Giddings et al., 2014). However, the existence of false negatives in this region suggests that while particles may not have reached the beach in this region because of the Columbia River plume in the model, *PN* cells were reaching these beaches under similar conditions. Previous studies suggest that it is often a race between the Columbia River plume and the upwelling front to reach beaches first during these wind reversals from upwelling to downwelling (Austin and Lentz, 2002; Giddings et al., 2014). It is possible that *PN* cells were able to beat the plume to the coast by a three-dimensional mechanism that is not well-captured by the model.

Similarly, while it is true that the *PN* abundance is not necessarily indicative of toxicity (Trainer et al., 2009) and thus the overall beached particle count may not be as important, defining a beaching event based on a threshold of 1 particle beaching within 0.125° of latitude per day is perhaps too lenient. As part of their efforts to reduce false positives, Giddings et al. (2014) applied a threshold of 10 particles in 20 days within their 0.4° latitude band before it would be considered a beaching event. Still, based on how forecasts are used to make sampling decisions, our stakeholders suggest that it is more important to know whether some number of particles will beach and where, than know if a big beaching event is expected. Future work should include testing of various particle count and length of beaching window, to arrive at a forecast model that is both more realistic and more accurate. Incorporating the results of this study as well as those from suggested future work will allow for better tailoring of the forecasts and information that they provide to fit the needs of our stakeholders.

Lastly, there are some caveats about the assumptions and the observational record that bear mentioning. This analysis only considered summer beaching events from one source, the Juan de Fuca eddy (MacFadyen et al., 2005; MacFadyen and Hickey, 2010). *PN* cell beaching events in spring and early summer typically originate at Heceta Bank and follow different dynamics in their transport to the beach (Hickey et al., 2013). Furthermore, as discussed, a recent study of the unusual HAB event in 2015, unprecedented in its spatial extent and in its severity, raised the possibility of a diffuse offshore source of *PN* cells rather than the identified "hot spots" for *PN* cell accumulation and growth (McCabe et al., 2016). This event was linked to anomalously warm ocean conditions, suggesting that these types of events could become more prevalent in the future under climate change. Capturing similar events that do not originate in a known "hot spot" like the Juan de Fuca eddy or Heceta Bank may be more difficult and requires further investigation. Both offshore and beach monitoring remain crucial to refinement and elaboration of this forecast system.

5. Conclusions

The goal of this study was to help improve how the forecasting model is used in the PNW HAB Bulletin's preparation by testing the model beaching definition and observational threshold used in the model for HABs that originate in the Juan de Fuca eddy, based on particle tracking experiments in the model combined with observations of beach *PN* cell counts. The results of this analysis suggest that:

1 *A narrower, more realistic definition of particle beaching works best statistically, but only in a sufficiently high-resolution (500 m), realistic (19 coastal rivers) version of the model.*
2 *Choice of beaching definition and observational threshold is largely dependent on the needs of the stakeholder.*

While these results are specific to the forecasting model used in the PNW HAB Bulletin project, they can also be used to inform other HAB forecasting models. The comparison of results within the medium-resolution version with those of the high-resolution version highlighted the importance of using a higher resolution model that includes coastal rivers, while also providing guidance on more appropriate beaching definitions to use with a lower resolution model. Still, the results of this study provide many avenues for future work in understanding transport pathways of HABs to the Pacific Northwest coast, including testing different thresholds for particle beaching, as well as incorporating other HAB sources, like the retentive region at Heceta Bank, and expanding the analysis area beyond 46N – 48N in the summer months. Together, this work will provide more region-specific forecasts tailored to the needs of stakeholders that will better prepare Pacific Northwest communities for HAB impacts.

Data availability

Access to model run setup files and derived output used for the particle tracking experiments in this paper are available upon request, without undue reservation, as described here: iodlabs.ucsd.edu/sgiddings/PNWTOX/contact.html and here: http://faculty.washington.edu/pmacc/LO/LiveOcean.html. These model setup files and output data are curated by MacCready on MacCready's server at UW and will remain curated for at least 5 years. ORHAB data are available upon request from orhab@uw.edu. ODFW data are available by submitting a request at https://www.dfw.state.or.us/agency/public_record/request.asp

Declaration of Competing Interest

The authors declare that they have no known competing financial interests or personal relationships that could have appeared to influence the work reported in this paper.

Acknowledgments

Special thanks to the MacCready and Banas lab groups for useful conversations; to collaborators in the PNW HAB Bulletin, particularly Barbara M. Hickey; to Raphael Kudela for useful comments; to Evelyn Lessard for guidance; and to David Darr for computer cluster administration and support. H. Stone was supported by a National Science Foundation (NSF) Graduate Research Fellowship. P. MacCready, N.

Banas, and H. Stone were supported by Monitoring and Event Response for Harmful Algal Blooms (MERHAB) grant number NA16NOS4780189 from the Coastal Ocean Program of the National Oceanic and Atmospheric Administration (NOAA). PM was also supported by the IOOS regional association NANOOS, and the Washington Ocean Acidification Center. This is contribution 246 of the MERHAB program. The statements, findings, conclusions, and recommendations are those of the authors and do not necessarily reflect those of NSF, NOAA, or the Department of Commerce. The Olympic Region Harmful Algal Bloom (ORHAB) partnership has been funded since 2006, through a surcharge to Washington State shellfish and seaweed licenses as authorized by RCW 77.21.555. We thank ORHAB and its member partners for providing *Pseudo-nitzschia* cell counts used in this manuscript. The PNW HAB Bulletin was developed with more than 15 years of funding from the NOAA National Ocean Service, National Centers for Coastal Ocean Science (NCCOS) sponsored research programs, Ecology and Oceanography of Harmful Algal Blooms (ECOHAB), and Monitoring and Event Response for Harmful Algal Blooms (MERHAB). Additional funding and support were provided by National Science Foundation ECOHAB program, NOAA Oceans and Human Health Initiative, the Centers for Disease Control, University of Washington, Washington State Department of Health, Washington Department of Fish and Wildlife, Quinault Indian Nation, the Quileute Tribe, and Makah Tribe.

References

Anderson, C.R., Sapiano, M.R.P., Prasad, M.B.K., Long, W., Tango, P.J., Brown, C.W., Murtugudde, R., 2010. Predicting potentially toxigenic Pseudo-nitzschia blooms in the Chesapeake Bay. J. Mar. Syst. 83 (3–4), 127–140. https://doi.org/10.1016/j.jmarsys.2010.04.003.

Anderson, C.R., Kudela, R.M., Kahru, M., Chao, Y., Rosenfeld, L.K., Bahr, F.L., et al., 2016. Initial skill assessment of the California harmful algae risk mapping (C-HARM) system. Harmful Algae 59, 1–18. https://doi.org/10.1016/j.hal.2016.08.006.

Anderson, D.M., Fensin, E., Gobler, C.J., Hoeglund, A.E., Hubbard, K.A., Kulis, D.M., et al., 2021. Marine harmful algal blooms (HABs) in the United States: History, current status and future trends. Harmful Algae 102, 101975. https://doi.org/10.1016/j.hal.2021.101975.

Austin, J.A., Lentz, S.J., 2002. The inner shelf response to wind-driven upwelling and downwelling. J. Phys. Oceanogr. 32 (7), 2171–2193. https://doi.org/10.1175/1520-0485(2002)032<2171:TISRTW>2.0.CO;2.

Banas, N.S., MacCready, P., Hickey, B.M., 2009. The Columbia River plume as cross-shelf exporter and along-coast barrier. Cont. Shelf Res. 29 (1), 292–301. https://doi.org/10.1016/j.csr.2008.03.011.

Banas, N.S., Conway-Cranos, L., Sutherland, D.A., MacCready, P., Kiffney, P.M., Plummer, M., 2015. Patterns of river influence and connectivity among subbasins of puget sound, with application to bacterial and nutrient loading. Estuaries Coast 38 (3), 735–753. https://doi.org/10.1007/s12237-014-9853-y.

Barron, C.N., Kara, A.B., Martin, P.J., Rhodes, R.C., Smedstad, L.F., 2006. Formulation, implementation and examination of vertical coordinate choices in the global navy coastal ocean model (NCOM). Ocean Model. 11, 347–375. https://doi.org/10.1016/j.ocemod.2005.01.004.

Barron, C.N., Smedstad, L.F., Dastugue, J.M., Smedstad, O.M., 2007. Evaluation of ocean models using observed and simulated drifter trajectories: impact of sea surface height on synthetic profiles for data assimilation. J. Geophys. Res. 112, 1–11. https://doi.org/10.1029/2006JC003982.

Barth, J.A., Menge, B.A., Lubchenco, J., Chan, F., Bane, J.M., Kirincich, A.R., et al., 2007. Delayed upwelling alters nearshore coastal ocean ecosystems in the northern California current. Proc. Natl. Acad. Sci. U. S. A. 104 (10), 3719–3724. https://doi.org/10.1073/pnas.0700462104.

Brasseale, E., Grason, E.W., McDonald, P.S., Adams, J., MacCready, P., 2019. Larval transport modeling support for identifying population sources of European green crab in the Salish sea. Estuaries Coast 42, 1586–1599. https://doi.org/10.1007/s12237-019-00586-2.

Brink, K.H., 2016. Cross-shelf exchange. Annu. Rev. Mar. Sci. 8 (1), 59–78. https://doi.org/10.1146/annurev-marine-010814-015717.

Davies, A.M., Xing, J, 2001. Modelling processes influencing shelf edge currents, mixing, across shelf exchange, and sediment movement at the shelf edge. Dyn. Atmos. Ocean 34, 291–326. https://doi.org/10.1016/s0377-0265(01)00072-0.

Davis, K.A., Banas, N.S., Giddings, S.N., Siedlecki, S.A., MacCready, P., Lessard, E.J., et al., 2014. Estuary-enhanced upwelling of marine nutrients fuels coastal productivity in the U.S. Pacific Northwest. J. Geophys. Res. Oceans 119 (12), 8778–8799. https://doi.org/10.1002/2014JC010248.

Denman, K.L., Freeland, H.J., 1985. Correlation scales, objective mapping and a statistical test of geostrophy over the continental shelf. J. Marine Res. 43 (3), 517–539. https://doi.org/10.1357/002224085788440402.

Freeland, H.J., Denman, K.L, 1982. Topographically controlled upwelling center off southern Vancouver Island. J. Marine Res. 40.

Freeland, H.J., McIntosh, P., 1989. The vorticity balance on the southern British Columbia continental shelf. Atmosphere Ocean 27 (4), 643–657. https://doi.org/10.1080/07055900.1989.9649359.

Giddings, S.N., MacCready, P., Hickey, B.M., Banas, N.S., Davis, K.A., Siedlecki, S.A., et al., 2014. Hindcasts of potential harmful algal bloom transport pathways on the Pacific Northwest coast. J. Geophys. Res. Oceans 119 (4), 2439–2461. https://doi.org/10.1002/2013JC009622.

Hallegraeff, G.M., Aligizaki, K., Amzil, Z., Anderson, P., Anderson, D.M., Arneborg, L., et al., 2021. Global HAB Status Report. A Scientific Summary for Policy Makers. UNESCO. (IOC Information Document, 1399.), Paris.

Hickey, B.M., Trainer, V.L., Michael Kosro, P., Adams, N.G., Connolly, T.P., Kachel, N.B., Geier, S.L., 2013. A springtime source of toxic pseudo-nitzschia cells on razor clam beaches in the pacific northwest. Harmful Algae 25, 1–14. https://doi.org/10.1016/j.hal.2013.01.006.

Lefebvre, K.A., Bargu, S., Kieckhefer, T., Silver, M.W., 2002. From sanddabs to blue whales: the pervasiveness Of domoic acid. Toxicon 40 (7), 971–977. https://doi.org/10.1016/s0041-0101(02)00093-4.

Lentz, S.J., Fewings, M.R., 2012. The wind- and wave-driven inner-shelf circulation. Ann. Rev. Mar. Sci. 4 (1), 317–343. https://doi.org/10.1146/annurev-marine-120709-142745.

Lévy, M., Ferrari, R., Franks, P.J.S., Martin, A.P., Rivière, P., 2012. Bringing physics to life at the submesoscale. Geophys. Res. Lett. 39 (14), 1–14. https://doi.org/10.1029/2012GL052756.

MacCready, P., McCabe, R.M., Siedlecki, S.A., Lorenz, M., Giddings, S.N., Bos, J., et al., 2021. Estuarine circulation, mixing, and residence times in the Salish sea. J. Geophys. Res. Oceans 126 (2). https://doi.org/10.1029/2020JC016738.

MacFadyen, A., Hickey, B.M., 2010. Generation and evolution of a topographically linked, mesoscale eddy under steady and variable wind-forcing. Continental Shelf Res. 30 (13), 1387–1402. https://doi.org/10.1016/j.csr.2010.04.001.

MacFadyen, A., Hickey, B.M., Foreman, M.G.G., 2005. Transport of surface waters from the Juan de Fuca eddy region to the Washington coast. Cont. Shelf Res. 25 (16), 2008–2021. https://doi.org/10.1016/j.csr.2005.07.005.

MacFadyen, A., Hickey, B.M., Cochlan, W.P., 2008. Influences of the Juan de Fuca Eddy on circulation, nutrients, and phytoplankton production in the northern California current system. J. Geophys. Res. Oceans 113 (8), 1–19. https://doi.org/10.1029/2007JC004412.

McCabe, R.M., Hickey, B.M., Kudela, R.M., Lefebvre, K.A., Adams, N.G., Bill, B.D., et al., 2016. An unprecedented coastwide toxic algal bloom linked to anomalous ocean conditions. Geophys. Res. Lett. 43 (19), 10366–10376. https://doi.org/10.1002/2016GL070023.

McKibben, S.M., Watkins-Brandt, K.S., Wood, A.M., Hunter, M., Forster, Z., Hopkins, A., et al., 2015. Monitoring Oregon Coastal Harmful Algae: Observations and implications of a harmful algal bloom-monitoring project. Harmful Algae 50, 32–44. https://doi.org/10.1016/j.hal.2015.10.004.

McKibben, S.M., Peterson, W., Wood, A.M., Trainer, V.L., Hunter, M., White, A.E., 2017. Climatic regulation of the neurotoxin domoic acid. Proc. Natl. Acad. Sci. 114 (2), 239–244. https://doi.org/10.1073/pnas.1606798114.

Noble, M., Jones, B., Hamilton, P., Xu, J., Robertson, G., Rosenfeld, L., Largier, J., 2009. Cross-shelf transport into nearshore waters due to shoaling internal tides in San Pedro Bay, CA. Contin. Shelf Res. 29 (15), 1768–1785. https://doi.org/10.1016/j.csr.2009.04.008.

Pierce, S.D., Barth, J.A., Thomas, R.E., Fleischer, G.W., 2006. Anomalously warm July 2005 in the northern California Current: Historical context and the significance of cumulative wind stress. Geophys. Res. Lett. 33 (22), L22S04. https://doi.org/10.1029/2006GL027149.

Ritzman, J., Brodbeck, A., Brostrom, S., McGrew, S., Dreyer, S., Klinger, T., Moore, S.K., 2018. Economic and sociocultural impacts of fisheries closures in two fishing-dependent communities following the massive 2015 U.S. West Coast harmful algal bloom. Harmful Algae 80, 35–45. https://doi.org/10.1016/j.hal.2018.09.002.

Shchepetkin, A.F., McWilliams, J.C., 2005. The regional oceanic modeling system (ROMS): a split-explicit, free-surface, topography-following-coordinate oceanic model. Ocean Model. 9 (4), 347–404. https://doi.org/10.1016/j.ocemod.2004.08.002.

Siedlecki, S.A., Banas, N.S., Davis, K.A., Giddings, S.N., Hickey, B.M., MacCready, P., et al., 2015. Seasonal and interannual oxygen variability on the Washington and Oregon continental shelves. J. Geophys. Res. Oceans 120 (2), 608–633. https://doi.org/10.1002/2014JC010254.

Stone, H.B., Banas, N.S., MacCready, P., 2018. The effect of alongcoast advection on pacific northwest shelf and slope water properties in relation to upwelling variability. J. Geophys. Res. Oceans 123 (1), 265–286. https://doi.org/10.1002/2017JC013174.

Sutherland, D.A., MacCready, P., Banas, N.S., Smedstad, L.F., 2011. A model study of the salish sea estuarine circulation. J. Phys. Oceanogr. 41 (6), 1125–1143. https://doi.org/10.1175/2011JPO4540.1.

Trainer, V.L., Suddleson, M., 2005. Monitoring approaches for early warning of domoic acid events in Washington State. Oceanography 18 (SPL.ISS.2), 228–237. https://doi.org/10.5670/oceanog.2005.56.

Trainer, V.L., Hickey, B.M., Horner, R.A., 2002. Biological and physical dynamics of domoic acid production off the Washington coast. Limnol. Oceanography 47 (5), 1438–1446.

Trainer, V.L., Hickey, B.M., Lessard, E.J., Cochlan, W.P., Trick, C.G., Wells, M.L., et al., 2009. Variability of Pseudo-nitzschia and domoic acid in the Juan de Fuca eddy region and its adjacent shelves. Limnol. Oceanogr. 54 (1), 289–308. https://doi.org/10.4319/lo.2009.54.1.0289.

Varanasi, U., Trainer, V.L., Schumacker, E.J., 2021. Taking the long view for oceans and human health connection through community driven science. Int. J. Environ. Res. Public Health 18 (5), 1–11. https://doi.org/10.3390/ijerph18052662.